Transportation Geotechnics 65 (2026) 102357

Contents lists available at ScienceDirect

Transportation Geotechnics

journal homepage: www.elsevier.com/locate/trgeo

Assessment of railway earthworks using DAS based active MASW surveys

Muhammad Saqlain [a,*], Andrew Trafford [a], Qasim Khan [a], Ben Dashwood [b], Jonathan E. Chambers [b], Gavin Jessamy [c], Julian Harms [c], Shane Donohue [a]

[a] School of Civil Engineering, University College Dublin, Dublin, Ireland
[b] British Geological Survey, UK
[c] Network Rail, UK

ARTICLE INFO

Keywords:
DAS
Fibre optic sensing
MASW
Shear wave velocity
Time-lapse monitoring
Railway earthworks
Seasonal moisture variation

ABSTRACT

Clay filled railway embankments may be particularly vulnerable to seasonal moisture variations, which induce shrink-swell behaviour, reduce stiffness, and adversely affect serviceability. This study evaluates the potential of Distributed Acoustic Sensing (DAS) based multichannel analysis of surface waves (MASW) for both large-scale characterisation and monitoring of such infrastructure. An active DAS-based MASW survey was conducted along a 5.8 km section of railway in southern England using existing loose-tube telecommunication fibre housed in trackside concrete troughing. In addition, repeated active DAS-based MASW surveys were undertaken over a 13-month period at the Withy Beds embankment, a 350 m section within the same route, using a tight-buffered fibre buried along the mid-slope. Conventional geophone surveys were also used to validate the DAS derived measurements.

Strong agreement is observed between DAS and geophone derived phase velocity responses and resulting shear-wave velocity (Vs) profiles, despite slightly higher noise levels in the DAS data. A comparison of different fibre-optic cable installations indicates that, although cables housed in trackside troughing exhibit reduced signal amplitudes due to poorer ground coupling, the fundamental-mode dispersion response remains clearly identifiable, enabling reliable Vs estimation using existing telecommunications infrastructure. The 5.8 km survey demonstrates the capability of DAS-based MASW to resolve spatial variations in near-surface Vs associated with earthwork type and embankment mechanical property variations. Time-lapse monitoring at the Withy Beds embankment reveals pronounced seasonal variations in near-surface Vs, with lower velocities during winter/spring and higher velocities during drier summer periods. These variations correlate with independent measurements of volumetric water content, matric suction, and soil moisture deficit, highlighting the sensitivity of Vs to hydro-mechanical processes in high-plasticity clay fills. The results demonstrate that DAS-based MASW provides a robust and scalable approach potentially informing targeted engineering intervention of railway earthworks using existing fibre-optic infrastructure.

1. Introduction

The performance of railway earthworks, constructed in the late nineteenth and early twentieth centuries, are increasingly concerning in the UK [1], particularly in Southeast and Central England, where embankments were often constructed of unsuitable high-plasticity clay fills. Clays such as London, Gault, Weald, Oxford, Kimmeridge, and Reading Clays exhibit significant volumetric instability, making them susceptible to deformation and, in some cases, failure under cyclic climatic (wetting–drying) conditions [2]. The UK's climate, characterised by wet winters and dry summers, induces seasonal shrink-swell cycles, causing considerable vertical surface displacements in some areas [3]. These movements compromise railway infrastructure by imposing speed restrictions, increasing maintenance demands, and heightening the risk of structural failure [4]. Repeated moisture cycling and associated pore pressure fluctuations may also lead to progressive softening of clay slopes, resulting in cumulative reductions in stiffness and shear strength [5]. In addition, desiccation cracking that is initiated during drying and

* Corresponding author.
E-mail addresses: muhammad.saqlain@ucdconnect.ie (M. Saqlain), andrew.trafford1@ucd.ie (A. Trafford), qasim.khan@ucd.ie (Q. Khan), bendas@bgs.ac.uk (B. Dashwood), jecha@bgs.ac.uk (J.E. Chambers), Gavin.Jessamy@networkrail.co.uk (G. Jessamy), Julian.Harms@networkrail.co.uk (J. Harms), shane.donohue@ucd.ie (S. Donohue).

https://doi.org/10.1016/j.trgeo.2026.102357
Received 22 April 2026; Received in revised form 26 August 2026; Accepted 26 August 2026
Available online 27 August 2026
2214-3912/© 2026 The Author(s). Published by Elsevier Ltd. This is an open access article under the CC BY license (http://creativecommons.org/licenses/by/4.0/).

exacerbated by repeated wetting and drying cycles can create preferential pathways for water infiltration, elevating pore water pressures and reducing shear strength [6,7]. Over time, these processes degrade the engineering properties of railway embankments, reducing their long-term resilience [8].

Climate change is expected to exacerbate these challenges. Climate model projections indicate that the UK will experience more extreme climatic variability, with drier summers and wetter winters, intensifying moisture fluctuations in clay embankments. This increased climatic stress will likely amplify shrink-swell cycles, leading to structural deformation and a higher incidence of slope failures. However, it should also be noted that high suctions during summer months can temporarily enhance slope stability by increasing effective stress in clay soils. This dynamic interplay between seasonal weakening and strengthening mechanisms highlights the need for effective monitoring of embankment conditions, especially in moisture-sensitive materials like London Clay.

Seismic geophysical monitoring techniques have, over recent years, shown potential for geotechnical site characterisation and for assessing the condition of slopes and earthworks [9–14]. Non-intrusive seismic methods have proven to be effective for assessing embankment stiffness, and detecting moisture-induced changes [15–17]. In particular, the Multichannel Analysis of Surface Waves (MASW) technique is widely used to model subsurface profiles of shear wave velocity (Vs), directly related to the small strain shear modulus (G_{max}) by equation (1), where ρ is the bulk density [10,11,18–24].

$$G_{max} = \rho \cdot V_s^2 \quad (1)$$

Because Vs (and G_{max}) is sensitive to seasonal moisture variations, it serves as a potentially reliable indicator of temporal stiffness changes in clay embankments [10]. Recent studies have further demonstrated the application of extensive active MASW surveys for large-scale shear-wave velocity characterisation and spatial mapping of subsurface variability, highlighting their value for engineering site characterisation and interpretation [23,24].

This paper evaluates the application of active-source MASW using Distributed Acoustic Sensing (DAS) for earthworks assessment. First, DAS-derived MASW results are validated through direct comparison with conventional geophone-based active surveys. Second, the feasibility of using standard telecommunication dark fibres, installed within trackside concrete troughing, as extended sensing elements for DAS-based MASW surveys, is assessed. Third, repeated DAS-based MASW surveys conducted over a 13-month period are used to monitor seasonal variations in Vs within a railway embankment in southern England. This extended monitoring period enables assessment of seasonal changes in embankment stiffness, while the distributed nature of DAS measurements enables the spatial variability of these changes to be characterised along the embankment..

1.1. Distributed Acoustic Sensing (DAS)

Distributed Acoustic Sensing (DAS) is a fibre-optic technology that uses standard optical fibre cable to measure spatially averaged strain along its length. The majority of DAS systems operate on the principle of coherent optical time-domain reflectometry (COTDR) [25,26]. Laser pulses are injected into the optical fibre from an interrogator unit (IU). As each pulse propagates along the fibre, a small portion of the light is backscattered due to microscopic imperfections within the glass. By understanding the propagation velocity of light within the silica fibre [27] and applying precise time gating, it is possible to interrogate the characteristics of the backscattered light returning from different positions along the fibre. Multiple successive pulses of light then allows the strain at each location to be interrogated several thousand times per second, enabling the detection of seismically induced strain within the fibre [28,29].

The potential of DAS has been demonstrated across a range of applications, including oil and gas exploration [30,31], carbon sequestration [32], seismological research [33], micro-seismic monitoring [34], and ambient noise-based seismic monitoring [35–37]. In near-surface applications, DAS offers the potential for high-resolution strain measurements over considerable distances [37,38]. It supports both active and passive seismic methods for subsurface characterisation and infrastructure monitoring [13,39–42]. DAS has, however, rarely been used in time-lapse monitoring of near-surface Vs. Where it has been applied for this purpose, most studies have focused on short-term or induced changes [37].

2. Materials & methods

2.1. Site description

The study site consists of c. 5.8 km section of live railway track to the southwest of London on Network Rail's New Guildford line (Fig. 1a), between Oxshott (c.0.5 km Southwest of Oxshott station) and Withy Beds (c.0.7 km Northeast of Effingham Junction station). This section includes approximately 3.3 km of embankments and 1 km of cut slopes. The majority of earthworks along this section of railway were constructed in the 19th century, with embankments likely formed of locally derived fill materials, as was the common practice at that time. The section of track investigated here lies almost entirely within the London Clay Formation of the Thames Group (Fig. 1a), and it is therefore likely that the embankments comprise reworked London Clay. In its natural condition, London Clay is a high-plasticity, usually stiff over-consolidated marine clay, typically characterised by low permeability, high shrink–swell potential, and strength and stiffness that are sensitive to variations in moisture content and soil suction [43–45]. These properties make reworked London Clay susceptible to seasonal shrink–swell behaviour and progressive softening when subjected to repeated wetting and drying cycles. In recent years, earthworks along this railway line have experienced recurring serviceability issues associated with seasonal volume change, which have necessitated the periodic imposition of speed restrictions.

More detailed investigations were carried out on a c. 350 m long, c. 5 m high section of embankment located at Withy Beds, approximately 1 km north of Effingham Junction Station. A landslip previously occurred on the NE side of this embankment a number of years ago.

2.2. Fibre optic and geotechnical sensor layout

A Network Rail loose-tube telecommunication cable, housed within a trackside ground-coupled concrete trough, provided continuous DAS coverage along the 5.8 km section of the New Guildford Line under investigation (Fig. 1a). At the Withy Beds embankment, two additional fibre optic cables, one tight buffered and one loose tube, each approximately 350 m long, were buried in a shallow trench (~10 cm depth) along the shoulder of the embankment (Fig. 1b), within 0.5 m of and parallel to the trackside cable trough. In addition, a further ~ 350 m of tight-buffered fibre-optic cable was buried at mid-slope in a shallow trench. DAS data for all surveys were acquired using an Optasense ODH4 Interrogator Unit, installed in a Relocatable Equipment Building (REB) located near Oxshott.

The Withy Beds embankment was also equipped with soil moisture and matric suction sensors, specifically Teros-21 and 5TE (Meter Environment, formerly Decagon Devices, Inc., Pullman, WA, USA) at 5 locations (WB1-WB5) along the mid-slope of the embankment, as shown in Fig. 1b. These sensor pairs were spaced 66 m apart and buried at a depth of 0.5 m. Teros-21 sensors measured matric suction, while the 5TE sensors recorded volumetric water content (VWC). The 5TE sensors operate on a capacitance-based principle to estimate soil moisture and therefore require calibration for soil-specific dielectric properties [46,47]. Sensor outputs were corrected using previously published

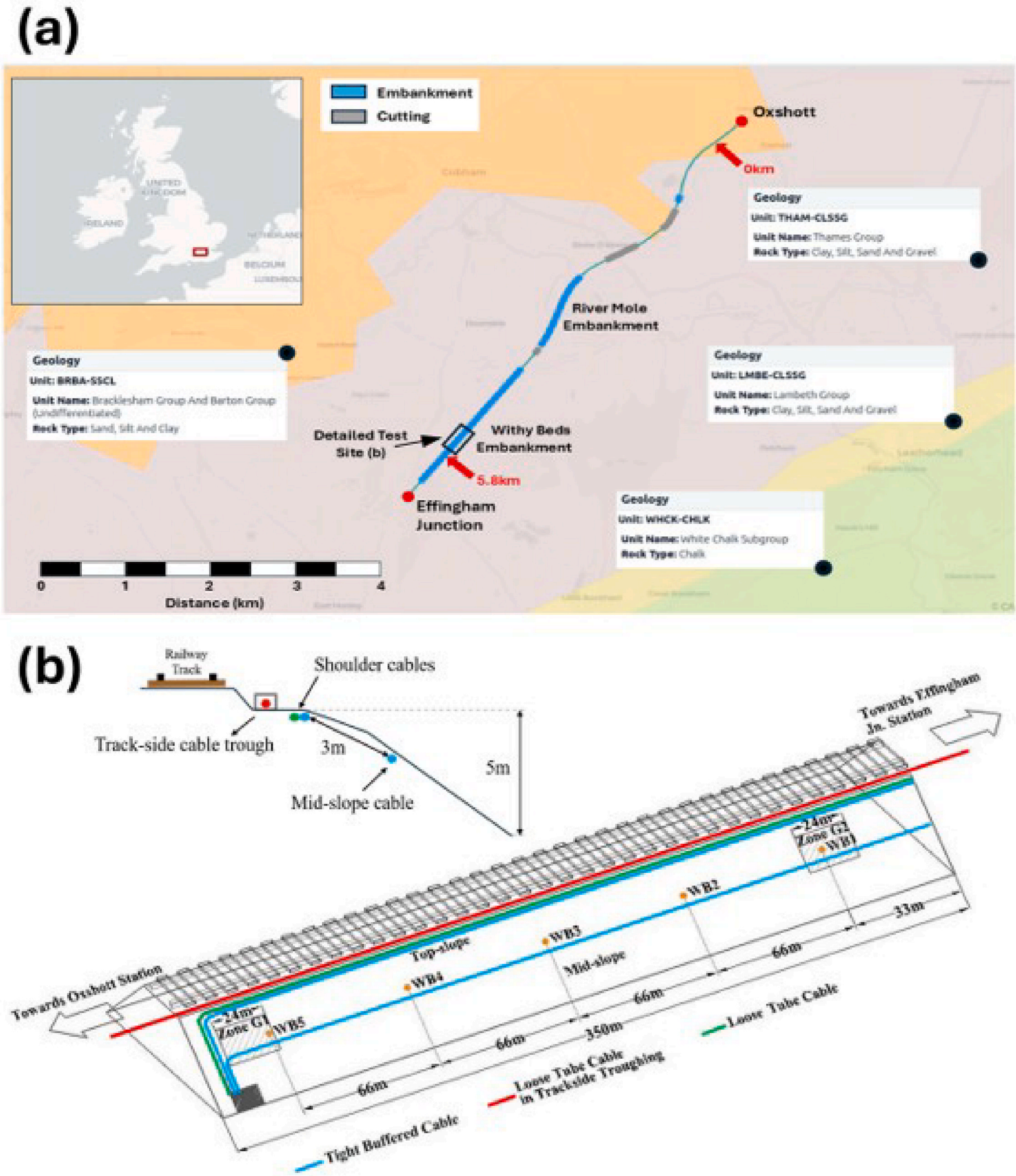

Fig. 1. (a) Section of the New Guildford Line between Oxshott station and Effingham Junction station in the Southeast of England, showing Network Rail earthwork assets (embankments and cuttings), overlain on a geological map of the area. Start and end points of the 5.8 km long DAS based MASW survey are indicated by red arrows. (b) cross section and 3D schematic of fibre-optic cable layout along the Withy Beds test embankment, including geophone survey locations (Zone G1-G2, 24 m each) and soil sensor locations (WB1-WB5). (For interpretation of the references to colour in this figure legend, the reader is referred to the web version of this article.)

calibration relationships developed specifically for the clay fill found at this site, as detailed in [48].

2.3. MASW data acquisition

2.3.1. Withy Beds mid-slope MASW surveys

In order to validate DAS-derived MASW results with respect to conventional geophone-based active surveys, parallel MASW DAS and geophone data were collected along the mid-slope of the railway embankment. Geophone data were acquired on Aug 23, 2022, and DAS data on Aug 24, 2022, using the same seismic source, with geophone and DAS channel locations co-located for each survey. As recommended by [49], a number of different source-receiver array geometries were assessed in order to determine the optimum MASW acquisition parameters. The geophone array consisted of 24, 4.5 Hz vertical geophones spaced at 1 m intervals and coupled to the ground using spiked metal plates to ensure firm contact. Geophone data were recorded, using a Geometrics Geode seismograph, at three different locations (Zone G1-G2) of the embankment, shown in Fig. 1b. DAS data were collected using the tight buffered cable shown in Fig. 1b, with a gauge length of 2 m and a channel spacing of 1 m. The sampling frequency was set to a minimum of 200 Hz for all surveys. The seismic source was a 1 kg hammer striking a metal plate, with an offset of 2 m. This offset was selected to maximise the recording of coherent high-frequency surface-wave energy required to resolve the upper few metres of the embankment. The lightweight hammer was selected to enhance the generation of high-frequency Rayleigh-wave energy and improve the resolution of the shallow embankment materials. A single hammer impact was recorded at each source location and no shot stacking was applied, as preliminary testing demonstrated that a single impact provided sufficient signal-to-noise ratio to produce clear Rayleigh-wave dispersion images over the frequency range of interest.

Repeat DAS based MASW surveys were subsequently carried out across the Withy Beds embankment over a 13-month period along the mid-slope of the embankment. Permanent markers were placed along the cable route to ensure consistent repeat source locations and alignment of the DAS channels across all surveys on the embankment. Data consistency was ensured by using the same sources, receivers, and recording equipment in each survey. Survey dates were: August 2022, November 2022, April 2023, and August 2023. For each of these surveys, shots were taken at 10 m intervals for the full length of the tight buffered mid-slope cable (c.350 m).

2.3.2. Oxshott-Withy Beds DAS based MASW survey

A 5.8 km long active MASW survey was conducted in November 2022 between Oxshott and Withy Beds. The survey primarily utilised a Network Rail loose-tube fibre-optic telecommunications cable housed within trackside ground-coupled concrete troughing. At the Withy Beds

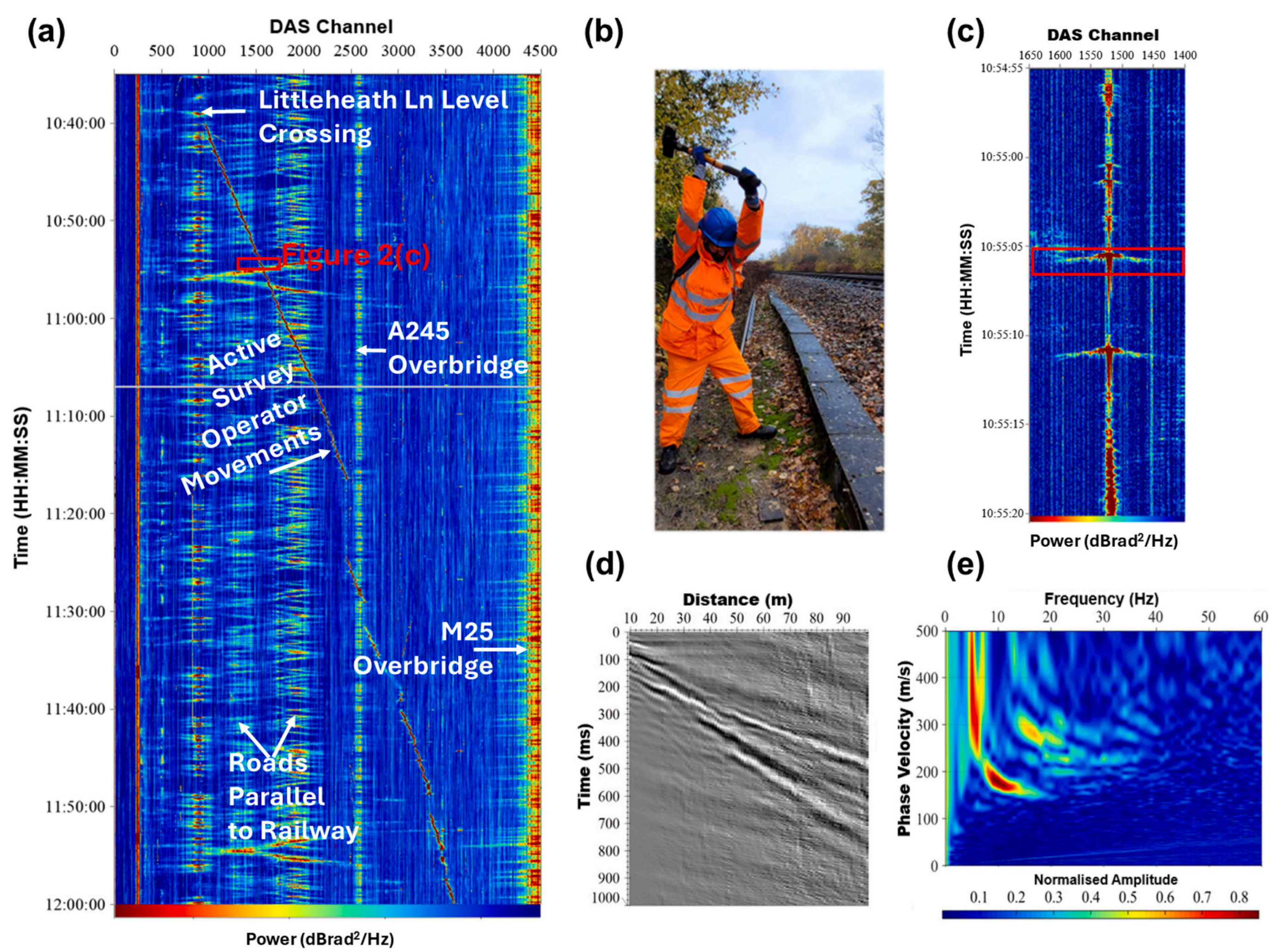

Fig. 2. (a) Annotated DAS Waterfall plot of 4.5 km of Network Rail troughing cable during active MASW survey, (b) picture of active survey being conducted showing concrete cable trough, (c) zoomed in portion of DAS waterfall plot (a), showing propagation of seismic waves along the cable from individual seismic shots, (d) corresponding seismic shot gather and (e) dispersion image.

embankment, located at the Southern end of the survey line, data were also recorded from the two additional fibre-optic cables (tight buffered and loose tube) buried in the embankment shoulder (Fig. 1b). These additional cables enabled the ground response recorded by three different cable configurations to be compared using a common seismic hammer source. This arrangement provided an opportunity to assess the feasibility of using standard trackside trough-installed telecommunications fibres for Vs profiling using MASW.

The survey was conducted during a line block, which allowed the track to be walked safely without train-related hazards. For this survey, a 4.5 kg sledgehammer and metal plate was used as the seismic source, with shots taken at 50 m intervals immediately beside the cable trough (Fig. 2b). Each dispersion image was generated using approximately 80 receiver channels with a 1 m channel spacing, corresponding to an analysis window of approximately 80 m. The selected 50 m shot spacing therefore provided substantial overlap between adjacent analysis windows while maintaining an appropriate balance between spatial resolution and survey efficiency for route-scale characterisation of the railway earthworks. At each location, two shots were acquired to assess repeatability, with the shot exhibiting the clearest coherent surface-wave response selected for subsequent processing and inversion. Shot locations were referenced using a GPS trigger that recorded location and time, enabling synchronisation with the DAS IU and facilitating accurate extraction of relevant seismic traces.

A real-time representation of the DAS data, known as a Frequency Bandwidth Extracted (FBE) waterfall plot, is shown in Fig. 2a. The FBE plot is generated by applying a Fast Fourier Transform to time-domain DAS data at each spatial channel and displaying the resulting phase spectral power density as a colour-coded frequency–distance map. Fig. 2a, covering the 5–55 Hz frequency band, represents a 1 h 15 min segment of the recorded DAS data and illustrates the progression of active survey operators from Oxshott towards Effingham Junction, together with prominent seismic noise such as a level crossing, overbridges (including the M25 motorway), and roads running parallel to the railway line. A zoomed-in section of the waterfall plot highlighting an individual seismic shot is shown in Fig. 2c. The shot generates a clearly identifiable seismic response, with coherent energy propagating along the fibre to approximately 100 m on either side of the shot point. The corresponding seismic shot gather and dispersion images are shown in Fig. 2d and 2e, respectively.

2.4. Data processing and inversion

Processing of the seismic surface wave data was performed by picking dispersion curves from a phase velocity-frequency spectra (dispersion image), generated using *MASWaves,* an open-source software [50]. The software applies a frequency-wavenumber (f-k) transformation to convert the time-domain data into the frequency phase velocity (f-ph) domain [51]. Dispersion curves were interpreted manually by a single experienced interpreter using a consistent picking procedure, as higher-mode energy and occasional ambiguity in identifying the fundamental mode in some datasets reduced the reliability of automated peak-picking methods.

In this study, a Monte Carlo Inversion (MCI) was employed to estimate the 1D Vs profile from the picked dispersion curves. MCI is a stochastic optimization technique that explores a predefined model parameter space through random sampling. The method is based on the multimodal misfit function approach introduced by [52] and [53], where a large number of models are generated against observed data to determine the optimal Vs profile. Following this framework, the inversion process involved estimating a single initial model, which was then applied for the Stochastic Monte Carlo (MC) inversion of surface wave data for all locations. This approach is based on the MC inversion algorithm described in [53]. Several initial models with different numbers of layers were evaluated to assess the robustness of the inversion and identify an appropriate model parameterisation. Following this procedure, the inversion model for the mid-slope MASW surveys was parameterised using five finite layers to a depth of 7 m, overlying an infinite half-space. Each layer was assigned a range of values for shear-wave velocity (Vs), P-wave velocity (Vp) and density (ρ). Dispersion curves were picked to the lowest coherent fundamental-mode frequency that could be reliably identified, with minimum picked frequencies typically between 10 and 15 Hz, corresponding to maximum wavelengths of approximately 15–17 m. Using the commonly adopted $\lambda/2$ relationship, these wavelengths correspond to an approximate effective investigation depth of 7.5–8.5 m. Consequently, the finite layers lie within the effective depth of investigation, whereas the underlying half-space is constrained primarily by the longest wavelengths and is therefore associated with greater uncertainty than the overlying finite layers. Vp was estimated by assuming a Poisson's ratio of 0.4, representative of unsaturated clay soil. Density values ranging from 1850 to 2000 kg/m3 were assigned to the individual layers and remained fixed during the inversion process. Vs and layer thickness were randomly varied by up to $\pm$ 5% from their initial values.

For the long active DAS-MASW survey, a larger 4.5 kg sledgehammer source generated coherent surface-wave energy over a broader frequency range, allowing the fundamental mode to be reliably picked to lower frequencies than for the mid-slope surveys. The maximum picked wavelength was approximately 24 m, corresponding to an approximate effective investigation depth of 12 m using the commonly adopted $\lambda/2$ relationship. Accordingly, the inversion model was parameterised using six finite layers overlying an infinite half-space, with the finite layers extending to approximately 12 m.

The MCI method involves generating random models, and those with misfit values below 2 were selected and averaged to obtain a final 1D velocity-depth profile. For each MC inversion, ten thousand iterations were performed using a fixed number of layer models. The final Vs profiles were obtained by averaging the velocity and depth of the accepted models, while the best-fit model was defined as the accepted model with the lowest misfit value. Fig. 3 illustrates a representative inversion result. Fig. 3a compares the observed dispersion picks with the theoretical dispersion curves generated from the accepted models, while Fig. 3b shows the distribution of accepted and rejected Vs models, with the averaged and best-fit profiles highlighted. The close clustering of the accepted models and the excellent agreement between the observed and theoretical dispersion curves indicate that the adopted inversion settings produced stable Vs profiles across the dataset.

3. Results and discussion

3.1. Comparison of DAS and geophone data

A comparison of dispersion curves, obtained using DAS and geophones at two locations on the Withy Beds embankment (Zones G1 and G2, see Fig. 1b), is shown in Fig. 4. DAS monitors the spatially averaged axial strain (or strain rate) over a gauge length, whereas geophones measure particle velocity at a point [54]. Despite the different physical quantities measured by each sensor type, the dispersion images show a reasonable degree of consistency across the two acquisition methodologies.

As reported previously [29,55,56], DAS dispersion images may exhibit enhanced sensitivity to higher-mode surface waves when compared with the geophone data, which more evident here in Fig. 4b than Fig. 4e. Although the fundamental mode is present in the DAS results, it is less distinct than in the geophone-derived dispersion images, reflecting the higher noise sensitivity of DAS, particularly at high frequencies. This is partly attributable to the finite gauge length of the DAS measurements, which effectively averages the recorded strain over the gauge length and can reduce the sharpness of the dispersion image, particularly at higher frequencies [56–59]. Nevertheless, at each location, the fundamental mode was identifiable and could be reliably picked in both DAS and geophone datasets. The comparison also

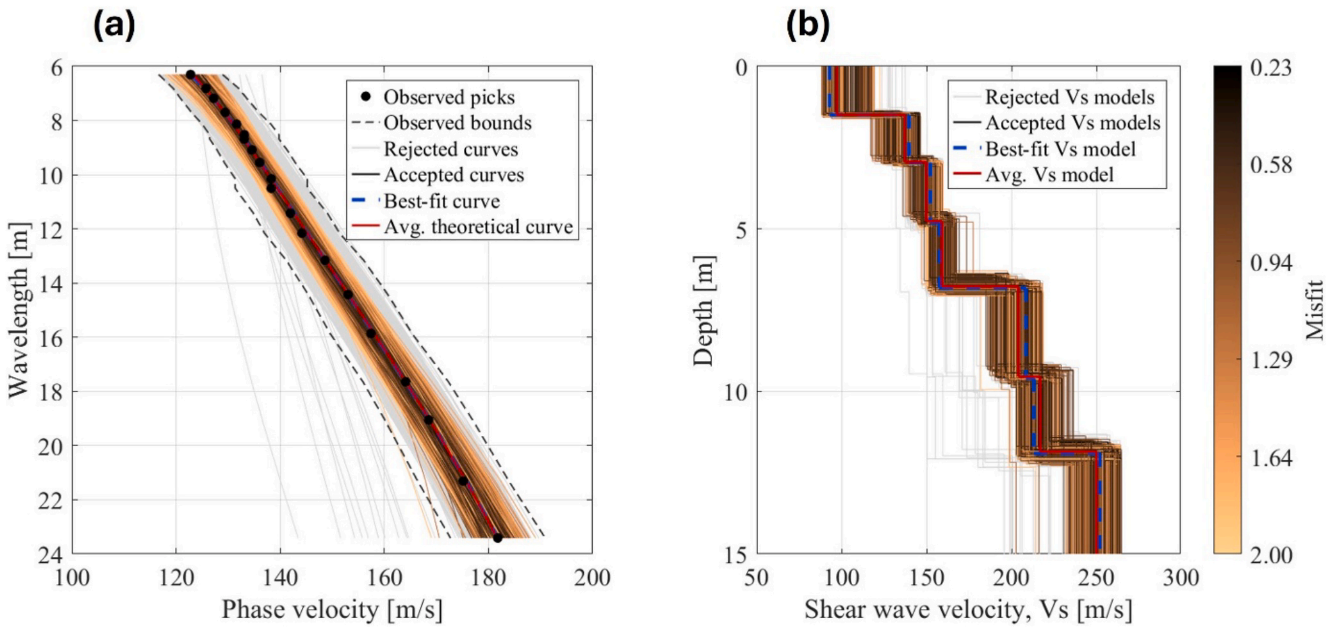

Fig. 3. Inversion result for the location approximately 3570 m from Oxshott (a) Observed dispersion picks and theoretical dispersion curves generated from the inversion. (b) Accepted and rejected Vs models. The best-fit and averaged models are highlighted, and the colour scale represents model misfit.

highlights differences at lower frequencies. While the geophone data generally exhibit stronger low-frequency energy, identification of the fundamental mode was not always straightforward because higher-mode energy became dominant in some datasets. Consequently, increasing uncertainty in identifying the fundamental mode was evident at the lowest frequencies in some of the DAS and geophone dispersion images.

Overall, geophone data display more stable phase velocities across the analysed frequency range, while DAS shows increased variability at higher frequencies. Despite observed differences in the dispersion images, strong agreement in fundamental mode phase velocity trends is observed (Fig. 4c, f). The quantitative comparison showed mean absolute percentage differences of 4.9% at G1 and 2.2% at G2, demonstrating that, in this case, DAS provides a viable alternative to geophones for surface-wave analysis at frequencies less than approximately 30–35 Hz, with the potential benefit of enhanced sensitivity to higher-mode energy.

3.2. Comparison of cable types

Prior to undertaking an extended active surface-wave survey alongside the trackside concrete cable trough, an assessment was carried out to evaluate the suitability of the existing fibre-optic cable for use in the survey. The cables are positioned within the trough alongside other cables and are therefore not optimally coupled to the ground. This raised concerns regarding their potential sensitivity for active Multichannel Analysis of Surface Waves (MASW) measurements.

When compared to the tight buffered and loose tube cables buried in a shallow trench adjacent to the concrete cable trough, the shot records (Fig. 5a, b, c) demonstrate, as expected, that the loose tube cable located within the concrete trough exhibits the lowest sensitivity. In contrast, the tight-buffered cable records the highest amplitude response of the three cable types (Fig. 5d). Phase velocity–frequency images derived from the shot gathers (Fig. 5e, f, g) indicate negligible differences between the loose-tube and tight-buffered cables within the frequency band corresponding to the fundamental mode generated by the hammer source.

Although the loose-tube cable located in the trackside concrete trough exhibits a substantial reduction in amplitude across the full frequency range for this shot gather (Fig. 5d), only a small reduction is observed in the frequency range over which the fundamental mode can be reliably identified and picked in the dispersion image (Fig. 5e). As all three shot gathers were recorded simultaneously from a single hammer impact, and the relative amplitudes do not decrease systematically with increasing distance from the interrogator unit, the observed differences are attributed primarily to cable construction and installation conditions rather than attenuation along the optical fibre. Consequently, despite reduced signal amplitude resulting from poorer ground coupling, the cable within the trough still retains sufficient sensitivity associated with picking of the fundamental surface-wave mode. However, the trough-installed cable exhibits a narrower usable frequency bandwidth, with coherent surface-wave energy visible up to around 16 Hz, compared with approximately 25 Hz for the shoulder-installed fibres. This reduction in usable frequency bandwidth limits the shortest resolvable wavelengths and therefore reduces the resolution of the shallowest part of the Vs profile.

3.3. Long active (5.8 km) DAS survey (Oxshott-Withy Beds)

One-Dimensional inverted Vs profiles were combined to produce a 10 m deep, 2D subsurface image illustrating the spatial variation of Vs along the 5.8 km section of the New Guildford Line under investigation (Fig. 6a). As indicated in Fig. 6a, two sections of the sensing cable were elevated and not ground-coupled, consequently, data from these sections were unsuitable for analysis. The profile was topographically corrected using LiDAR data, which was available for the full survey length. The dashed line, indicates the natural ground level, 10 m to the Southeast of the railway line and so provide a good indication of the location of earthwork structures along the route, with elevated sections above the natural ground level indicative of embankments, and depressed sections below the natural ground level indicative of cuttings. The Network Rail earthwork classification is also shown at the base of Fig. 6a.

Marked contrasts in Vs are observed between earthwork types. Embankment sections exhibit substantially lower velocities (Vs ≈ 80–120 m/s) than adjacent cuttings, where velocities commonly exceed 140 m/s. This contrast is consistent with the expected difference in stiffness between the relatively undisturbed London Clay underlying the

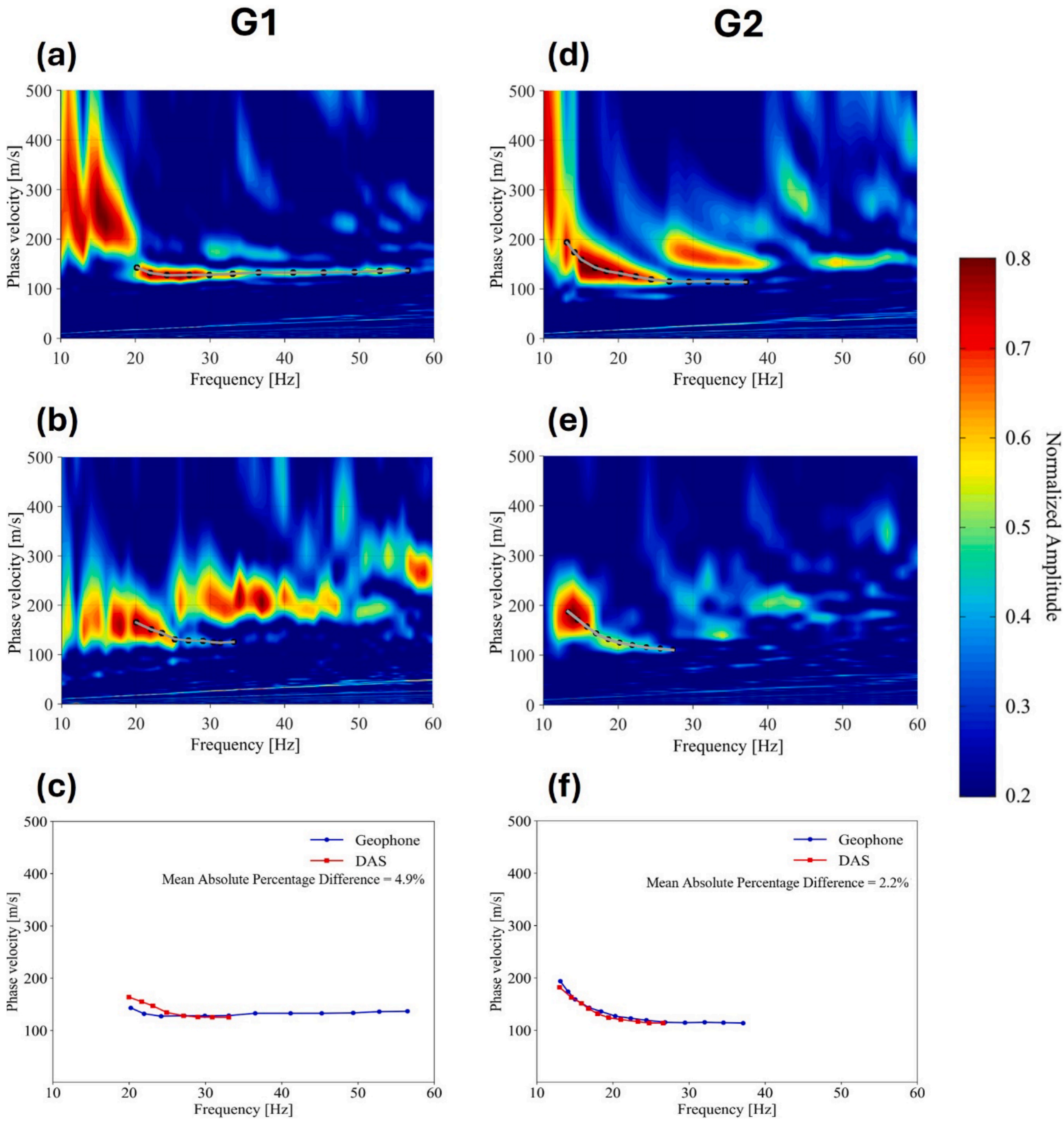

Fig. 4. Dispersion images acquired using geophones (panels a,d) and DAS (panels b,e) at two locations on the Withy Beds embankment, G1 and G2 (Fig. 1b). Panels c, and f provide a comparison of corresponding picked dispersion curves (fundamental mode only) from the two locations.

cutting sections and the reworked, often heterogeneous clay fill that forms the embankments. However, localised Vs variations within cutting sections should be interpreted with caution, as the survey sampled the railway corridor rather than the slope face directly. An exception to the general trend is observed near the M25, where comparatively low Vs values occur within a cutting. Without site-specific geotechnical, drainage or asset condition information, the cause of this anomaly cannot be determined, although it may reflect local geological variability, drainage conditions or localised deterioration of the earthwork. For Fig. 6c presents the average Vs within the upper 2 m overlain on LiDAR-derived topography, highlighting the transition between the River Mole embankment and the adjacent cutting. This contrast reflects the differing condition of reworked embankment fill and intact natural clay. Despite more than a century of ageing, the persistently lower Vs values within embankment sections indicate comparatively soft ground conditions, highlighting the ongoing vulnerability of these structures. Localised variations in Vs within embankments on this route are also observed and this is likely due to the heterogeneous nature of the embankment fill, which was typically constructed from locally sourced materials of variable composition and condition. The ability of DAS-based MASW to resolve softened zones and heterogeneous ground conditions is particularly useful in the context of embankment condition, as these spatial variations in small strain stiffness may influence deformation behaviour. Overall, these results demonstrate the

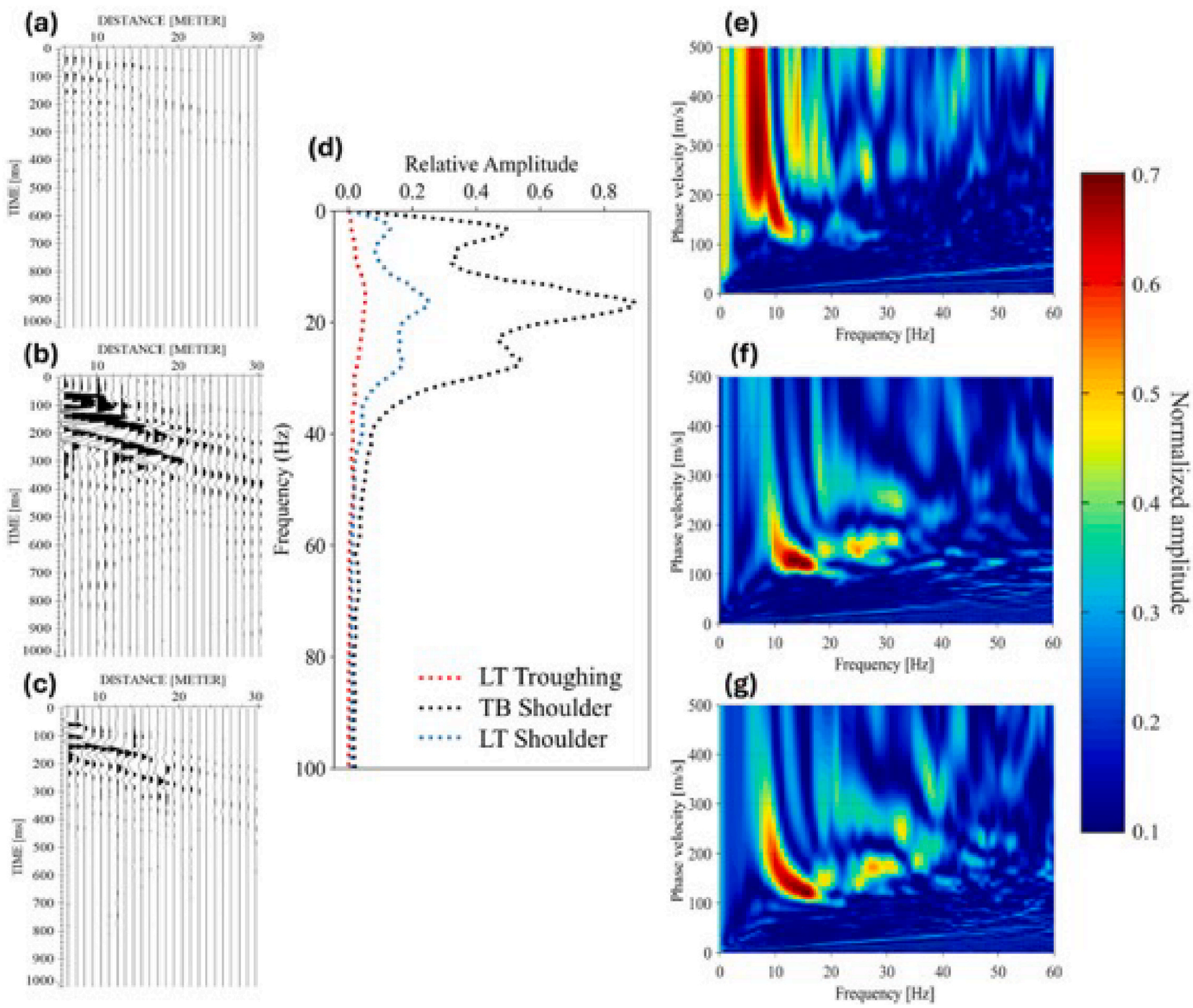

Fig. 5. Seismic shot gathers and corresponding dispersion images acquired using (a & e) a loose tube (LT) cable located in concrete troughing, (b & f) a tight buffered (TB) cable buried in the shoulder of the embankment, (c & g) a loose tube cable also buried in the shoulder. Relative amplitude vs frequency for each of the cable variants is shown in (d).

capability of DAS-based MASW to deliver near surface stiffness characterisation over long distances by utilising existing fibre-optic cables as a continuous seismic array. This approach overcomes the spatial limitations of conventional geophone deployments, enables dense, kilometre-scale mapping of subsurface stiffness, while also offering practical advantages for long-term monitoring through the use of permanently installed fibre-optic infrastructure, reduced field deployment requirements, and potentially lower operational costs than conventional geophone surveys.

3.4. Withy Beds embankment: independent sensor and SMD data

Hourly measurements from soil moisture and suction sensors located at 5 points along the embankment are illustrated in [48]. Data from Aug 2022 to Sep 2023 are shown, covering the periods during which active seismic surveys were conducted. As the sensors were installed at 0.5 m depth, they are sensitive to near-surface moisture conditions, and although some variability exists, all exhibited broadly similar responses ([48]). Data from VWC sensor WB4 is not shown, as the sensor malfunctioned. Also, due to power issues with the data loggers there are some data gaps from Jun 2023 to the end of the monitoring period.

The embankment exhibited clear seasonal moisture trends. VWC are highest and soil suction is lowest during winter and spring (Nov to May), with VWC ranging from 60 to 75% and suction approaching zero kPa. In contrast, drier conditions were observed during summer, with VWC decreasing 35–45% and suction increasing to values up to 1200 kPa at WB3. Some variability in moisture and suction response was noted between locations, likely reflecting subsurface heterogeneity.

Soil Moisture Deficit (SMD), for the same time period, is also presented in [48]. These data were obtained from the Met Office's Rainfall and Evapo-transpiration Calculation System (MORECS), which provides an average SMD over 40 km x 40 km squares covering the UK. These data show very high SMD was measured during the summer of 2022, approaching the highest Network Rail SMD threshold for this location (300 mm). This threshold is associated with a requirement for engineering interventions (e.g. speed restrictions) due to the potential for considerable volume change (shrinkage) associated with moisture loss in high plasticity clay soils. During the summer of 2023, the SMD level, while high (>175 mm), did not reach the same level as the previous summer.

3.5. Withy Beds embankment: active DAS based MASW monitoring

Example dispersion images obtained from active surveys conducted during four monitoring periods (August 2022, November 2022, April 2023 and August 2023), using the same seismic source and DAS receiver

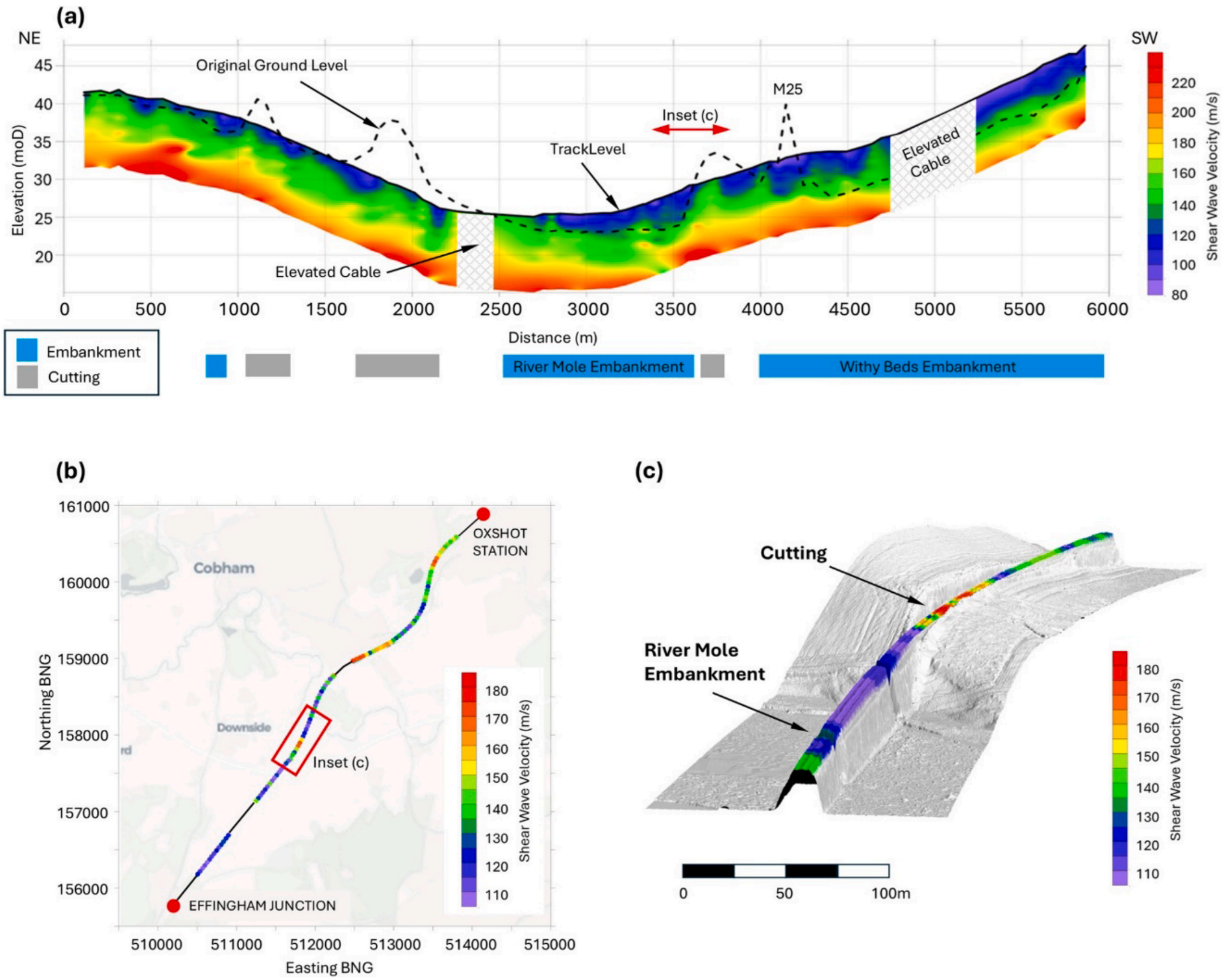

Fig. 6. (a) 5.8 km long DAS-based MASW profile of the New Guildford line between Oxshott and Withy Beds, showing the location of the various earthworks on the line, (b) average Vs within the upper 2 m for the full active survey length, (c) average Vs within the upper 2 m overlain on LiDAR-derived topography, showing the transition in Vs between the River Mole embankment and the adjacent cutting.

section along the embankment, are presented in Fig. 8a–d. A clear fundamental mode is identifiable in each dispersion image, and the corresponding picked dispersion curves for each survey are shown together in Fig. 8e for comparison. Distinct differences are evident between the curves, particularly at frequencies above approx. 15 Hz, where considerably lower phase velocities are observed in April 2023 compared with August 2022 and 2023. When dispersion curves from all active surveys across the full slope are plotted together (Fig. 8f), consistent spatio-temporal trends in phase velocity are apparent.

Time-lapse two-dimensional Vs profiles for the 350 m long Withy Beds embankment, derived from inversion of picked fundamental-mode dispersion curves from the four active DAS-based MASW surveys, are presented in Fig. 9(a–d), overlain on LiDAR-derived topographic information for the embankment. Clear temporal variations in near-surface Vs are evident, indicating a strong seasonal control on embankment stiffness. As expected from the picked dispersion curve data, the most pronounced changes occur in the near surface, within the upper 2–3 m, where soil properties are particularly sensitive to variations in moisture content and matric suction. Elevated Vs values were observed during the late summer surveys in August 2022 and August 2023, whereas substantially lower Vs values were recorded in November 2022 and April 2023. The average near-surface Vs differed by approximately 22% between the highest-velocity (August 2022) and lowest-velocity (April 2023) surveys. Based on the relationship between Vs and G_{max} (Equation (1), this 22% reduction in Vs corresponds to an approximate 39% reduction in G_{max} (assuming constant bulk density) within the upper 2–3 m of the embankment. This change is substantially greater than the variability typically reported for well-resolved surface-wave dispersion [60], supporting the interpretation that the observed temporal variations reflect seasonal changes in embankment stiffness rather than measurement uncertainty. These temporal variations are consistent with the seasonal moisture trends shown in Fig. 7 and are examined in more detail in the following section.

In addition to seasonal trends, significant lateral variability in Vs is observed along the length of the 2D profiles. Lateral variability is clearly illustrated in Fig. 9e, where near surface, inverted Vs (layer from 1-2 m depth) is presented for August 2022, representing the highest velocities recorded during the monitoring period, and April 2023, representing the lowest velocities. These data highlight the spatial extent of seasonal stiffness variations across the embankment. As described above, for the 5.8 km long active DAS survey, the observed variability at the Withy Beds embankment is likely influenced by the heterogeneous nature of the embankment fill. Differences in soil suction, recorded by sensors at separate locations along the embankment, further indicate lateral

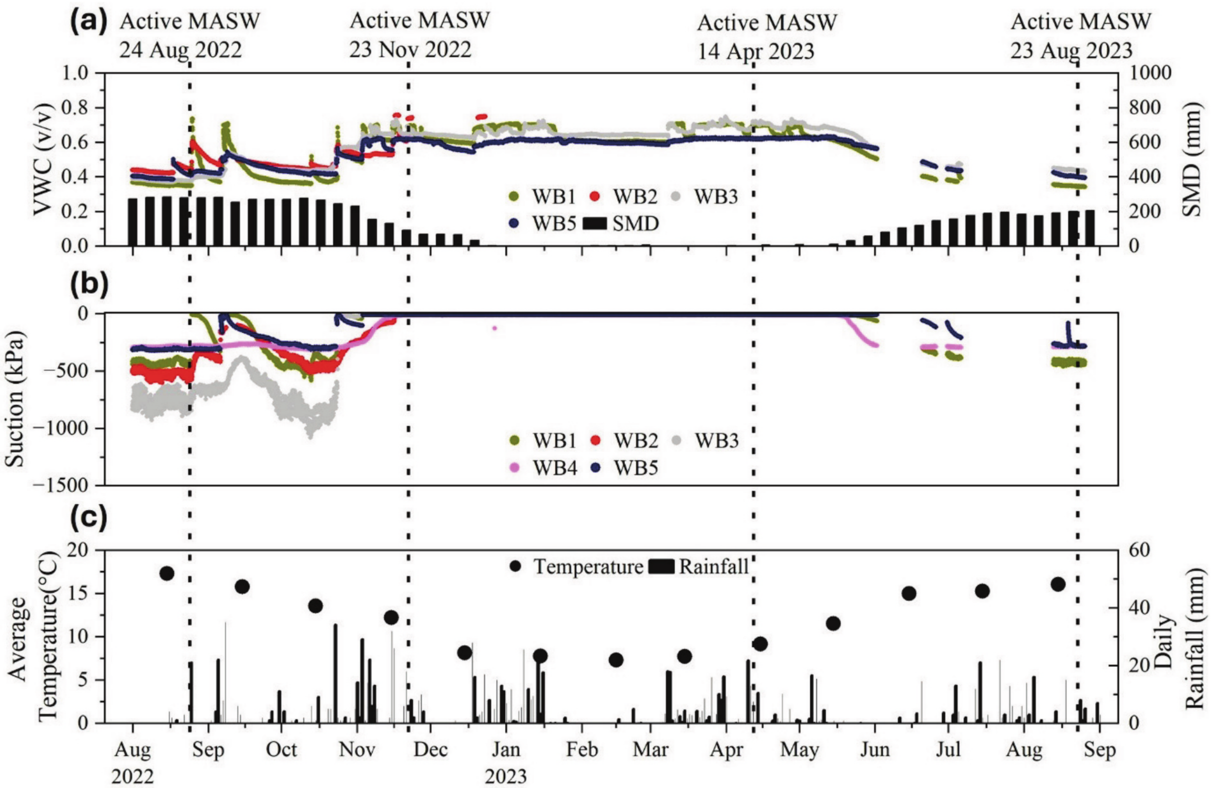

Fig. 7. Hourly sensor data between Aug 2022 and Aug 2023, (a) VWC data from 5TE sensor and Soil Moisture Deficit (SMD), (b) Suction sensors measurements, (c) Monthly average temperature and daily rainfall data.
Adapted from [48] .

variability in moisture regime and material response. The embankment is also densely vegetated, with several mature deciduous trees distributed along its length which, as noted by [61], can induce significant soil drying through evapotranspiration, increasing matric suction and effective stress in clay-rich embankments. The combined effects of material heterogeneity and vegetation-induced moisture variation likely contribute to the observed spatial variability in Vs, with localised zones of elevated stiffness occurring despite the generally low quality of the clay fill. While such vegetation-induced stiffening may temporarily increase Vs, it may also enhance shrink–swell behaviour and promote desiccation cracking, with potential implications for long-term embankment performance.

3.6. Relationship between shear-wave velocity and moisture conditions

Vs values derived from DAS measurements are plotted against VWC and soil suction in Fig. 10a and Fig. 10b respectively. Each Vs value corresponds to the location of an in-situ soil sensor and is paired with the average VWC and matric suction recorded on the day of the active geophysical survey. Although there is scatter in the data, reasonably clear relationships can be observed between the parameters. Together, these trends reflect moisture-induced changes in effective stress within the clay-rich embankment fill. Increasing water content lowers matric suction, reducing the effective stress acting within the soil skeleton and consequently decreasing small-strain stiffness and shear-wave velocity. [48,62,63]. Although this interpretation is consistent with published stress-dependent Vs relationships, a quantitative comparison was beyond the scope of the present study. Under seasonal wetting, repeated reductions in suction may contribute to cumulative degradation of stiffness, increasing the susceptibility of embankment slopes to deformation and delayed instability. Conversely, during drier periods elevated suction enhances soil stiffness and temporarily improves embankment stability, however, in high-plasticity clays this increase in suction is also associated with shrinkage-induced volume change, which can give rise to serviceability problems such as differential settlement, cracking, and track geometry defects. Over successive seasonal cycles, the alternating effects of wetting-induced softening and drying-induced shrinkage may promote progressive softening and strain accumulation within the embankment, particularly in these high-plasticity clay fills [64].

From an engineering perspective, these results demonstrate that seasonal variations in near-surface stiffness are sufficiently large to be detected using time-lapse DAS-based MASW and are therefore relevant to the assessment of railway earthworks. The technique has the potential to identify embankment sections exhibiting anomalously large or spatially variable seasonal stiffness changes, allowing these locations to be prioritised for detailed geotechnical investigation, targeted maintenance or more frequent monitoring. More broadly, these findings demonstrate the potential of distributed fibre-optic sensing to provide continuous, network-scale information on seasonal changes in embankment condition using existing telecommunications infrastructure, offering a level of spatial and temporal coverage that would be impractical to achieve using conventional site investigation techniques.

It is recognised that a limitation of this analysis arises from the disparity in measurement scale between the soil sensors and the MASW-derived Vs values. While the sensors sample a small, localised soil volume, the MASW Vs estimates represent an averaged response over a larger subsurface volume. In future studies, a denser network of moisture and suction sensors, including measurements at multiple depths, could better capture the spatial variability of moisture conditions within the embankment and may improve the correlation with MASW-derived Vs measurements. Additional uncertainty may arise from the assumption that the average daily VWC and suction measurements are representative of the moisture conditions governing the geophysical response

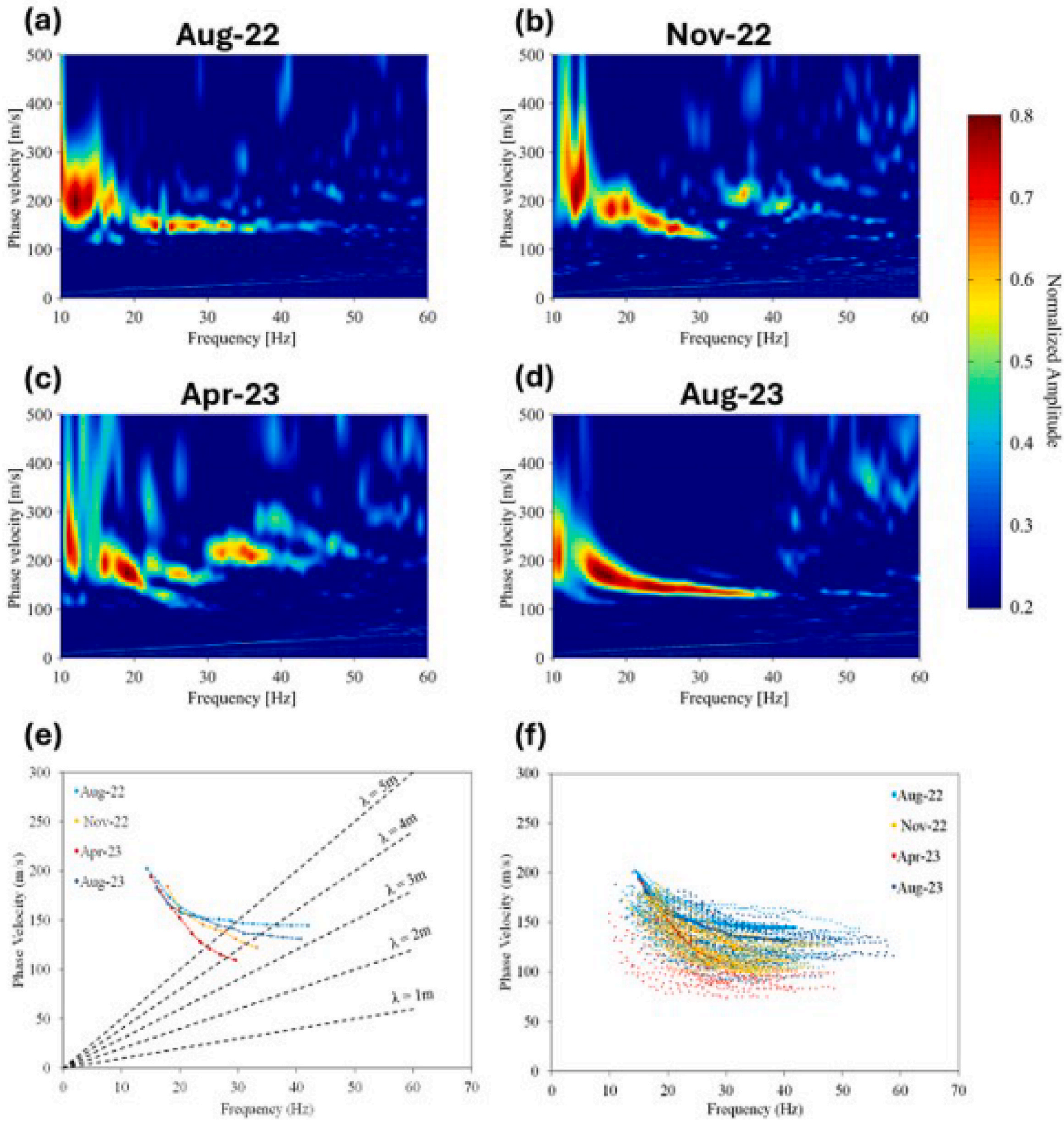

Fig. 8. Comparative dispersion analysis of surface waves across four survey periods. Panels (a)–(d) display the phase velocity frequency (Vph –f) spectra for surveys conducted in Aug-2022, Nov-22, Apr-23, and Aug-23 at a location approximately 125 m from the start of the cable. (e) shows the dispersion curves extracted from these four dispersion images. (f) presents a scatter plot of the picked dispersion points from all four surveys, to facilitate direct comparison of the seismic velocity characteristics over time.

at the time of acquisition as short-term fluctuations in moisture conditions may not be fully captured. Furthermore, all DAS measurements were acquired using a single gauge length (2 m), and only four repeat MASW surveys were conducted during the monitoring period. Future work could investigate the influence of DAS acquisition parameters and more frequent survey intervals on the observed Vs–moisture relationships. Despite these limitations, the consistent inverse relationship between Vs and moisture content, and the corresponding positive relationship between Vs and matric suction, provide field-scale evidence that DAS-based MASW is sensitive to the hydro-mechanical processes controlling seasonal stiffness variations in clay-rich railway embankments.

4. Conclusions

This study demonstrates the applicability of Distributed Acoustic Sensing (DAS) based multichannel analysis of surface waves (MASW) for the characterisation and monitoring of clay-filled railway embankments. Direct comparison with conventional geophone-based active surveys at the Withy Beds embankment validated the DAS-derived MASW results. The comparison demonstrated good agreement in the fundamental-mode phase-velocity trends, thereby confirming the reliability of the

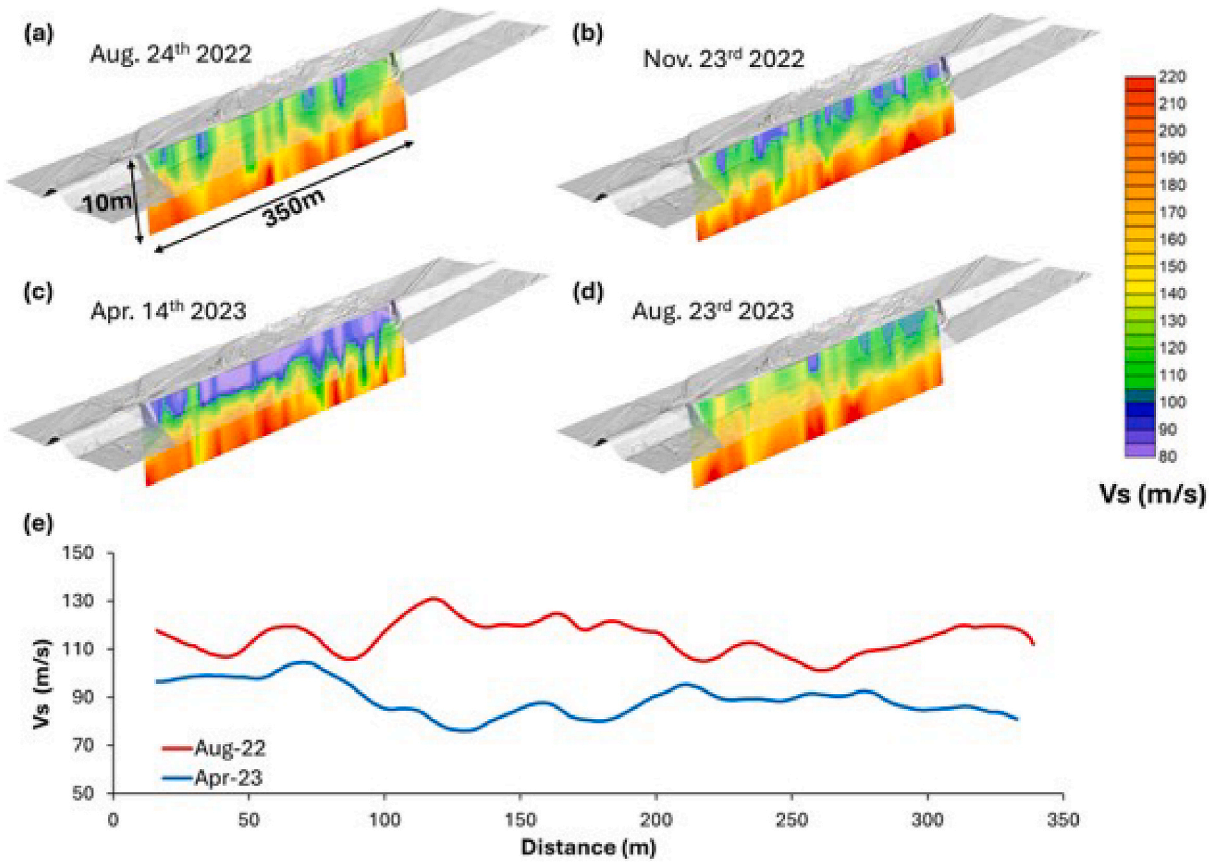

Fig. 9. Temporal variation in inverted two-dimensional shear-wave velocity (Vs) profiles along the 350 m-long Withy Beds embankment derived from active DAS-based MASW surveys conducted on four dates: (a) 24 August 2022, (b) 23 November 2022, (c) 14 April 2023, and (d) 23 August 2023. Panel (e) illustrates lateral variability in inverted Vs at 1 m depth for August 2022 (representing the highest velocities recorded during the monitoring period) and April 2023 (representing the lowest velocities).

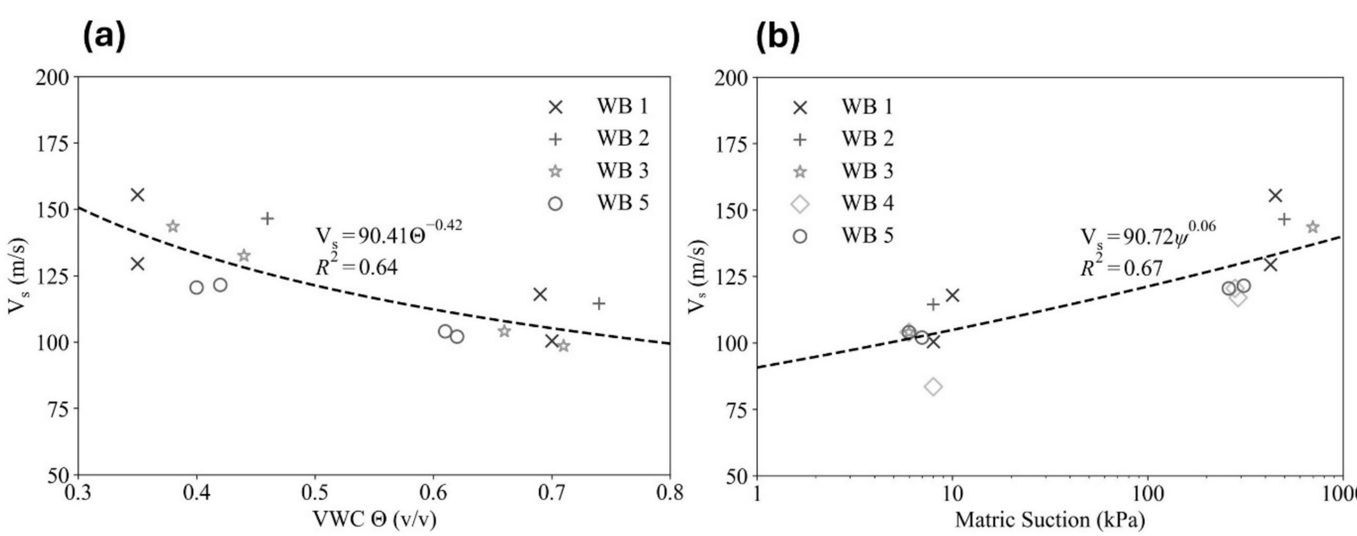

Fig. 10. Relationship between DAS-based Vs measurements and soil sensor data (a) VWC vs Vs (b) Matric Suction vs Vs.

DAS-derived shear-wave velocity (Vs) estimates.

Although DAS data exhibited higher noise levels, key seismic responses were consistently captured, validating DAS as a practical alternative to conventional geophone arrays.

Comparison of different fibre-optic cable configurations demonstrated that standard telecommunications cables installed within trackside concrete troughing exhibit lower signal amplitudes due to reduced ground coupling when compared with cables buried directly in the ground. However, despite this reduction in amplitude, the fundamental-mode dispersion response remains identifiable, indicating that standard trackside fibres can provide reliable data for MASW-based Vs profiling.

Application of DAS-based MASW profiling along a 5.8 km railway section between Oxshott and Withy Beds demonstrates the potential for large-scale earthworks assessment using this existing fibre-optic infrastructure. Two-dimensional Vs profiles clearly differentiate embankments from cuttings, with embankment sections exhibiting persistently lower velocities than adjacent cut slopes. These contrasts reflect differences between reworked clay fill and natural London Clay and indicate comparatively softened ground conditions within embankments. Localised near surface stiffness variations may also be associated with the heterogeneous nature of embankment fill in old earthworks, however variations associated with dense trackside vegetation were also noted, highlighting the influence of moisture regime and land cover on embankment behaviour.

Time-lapse DAS-based MASW surveys conducted over a 13-month period at the Withy Beds embankment revealed pronounced seasonal variations in near-surface stiffness, particularly within the upper 2–3 m. These variations were strongly correlated with independent measurements of volumetric water content, matric suction and soil moisture deficit, demonstrating a clear link between Vs and seasonal hydro-mechanical processes within the embankment. The combined use of distributed seismic observations and point-based sensor data provides insight into embankment behaviour across both spatial and temporal scales. While differences in measurement scale are likely to have introduced some scatter, the consistent seasonal patterns highlight the sensitivity of DAS-based MASW to the hydro-mechanical processes governing embankment performance. By enabling kilometre-scale, high-resolution stiffness mapping using existing fibre-optic infrastructure, this approach offers a potentially valuable tool for targeted condition assessment and long-term management of climate-sensitive railway earthworks.

CRediT authorship contribution statement

Muhammad Saqlain: Writing – review & editing, Writing – original draft, Visualization, Validation, Software, Methodology, Investigation, Formal analysis, Data curation, Conceptualization. **Andrew Trafford:** Writing – review & editing, Visualization, Validation, Software, Methodology, Investigation, Formal analysis, Data curation, Conceptualization. **Qasim Khan:** Writing – review & editing, Visualization, Validation, Methodology, Formal analysis, Conceptualization. **Ben Dashwood:** Resources, Methodology, Investigation. **Jonathan E. Chambers:** Resources, Methodology, Investigation. **Gavin Jessamy:** Supervision, Resources, Project administration. **Julian Harms:** Supervision, Resources, Project administration. **Shane Donohue:** Writing – review & editing, Visualization, Validation, Supervision, Project administration, Investigation, Funding acquisition, Formal analysis, Conceptualization.

Declaration of competing interest

The authors declare that they have no known competing financial interests or personal relationships that could have appeared to influence the work reported in this paper.

Acknowledgement

The first author (Saqlain) acknowledges iCRAG - the Research Ireland Centre in Applied Geosciences, for their funding, (iCRAG-Phase 2 – Grant Code: 13/RC/2092_P2). Trafford and Khan were funded with the financial support of Research Ireland, under the National Challenge Fund Programme grant 23/NCF/SC/11625.

Data availability

Data will be made available on request.

References

[1] Skempton AW. Embankments and cuttings on the early railways. 1996, The Civil Engineering of Canals and Railways.
[2] Driscoll R. The influence of vegetation on the swelling and shrinking of clay soils in Britain. Geotechnique 1983;33(2):93–105. https://doi.org/10.1680/geot.1983.33.2.93.
[3] Biddle G. Tree root damage to buildings, in Expansive clay soils and vegetative influence on shallow foundations. 2001. p. 1-23.
[4] Rail N. RSSB 1386 (revised) the effects of railway traffic on embankment stability. RSSB (Rail Safety and Standards Board); 2011.
[5] Skempton A. Long-term stability of clay slopes. Geotechnique 1964;14(2):77–102. https://doi.org/10.1680/geot.1964.14.2.77.
[6] Perry J. A survey of slope condition on motorway earthworks in. England and Wales; 1989.
[7] Anderson MG, Kneale PE. Pore water pressure and stability conditions on a motorway embankment. Earth Surf Processes 1980;5(1):37–46. https://doi.org/10.1002/esp.3760050105.
[8] Hulme M. Climate change scenarios for the United Kingdom: the UKCIP02 scientific report. 2002: Tyndall Centre for Climate Mental Sciences University.
[9] Gunn D, et al. Deterioration model and condition monitoring of aged railway embankment using non-invasive geophysics. Constr Build Mater 2018;170:668–78. https://doi.org/10.1016/j.conbuildmat.2018.03.066.
[10] Bergamo P, et al. Time-lapse monitoring of climate effects on earthworks using surface waves. Geophysics 2016;81(2):EN1–15. https://doi.org/10.1190/geo2015-0275.1.
[11] Bergamo P, et al. Time-lapse monitoring of fluid-induced geophysical property variations within an unstable earthwork using P-wave refraction. Geophysics 2016; 81(4):EN17–27. https://doi.org/10.1190/geo2015-0276.1.
[12] Saqlain M, et al. DAS based active seismic survey to monitor railway embankment performance under seasonal variation, in Civil Engineering Research in Ireland conference 2024 (CERI2024). 2024: Galway. p. 4.
[13] Trafford A, et al. Seasonal variation in railway embankment condition from passive analysis of train generated surface waves using DAS. NSG 2024 30th European Meeting of Environmental and Engineering Geophysics. European Association of Geoscientists & Engineers; 2024. 10.3997/2214-4609.202420179.
[14] Anshu AK, et al. Seismic site classification of Itanagar city, India, considering spatial variation of shear wave velocity obtained using extensive active MASW survey. J Appl Geophys 2025:105981. https://doi.org/10.1016/j.jappgeo.2025.105981.
[15] Whiteley J, et al. Geophysical monitoring of moisture-induced landslides: a review. Rev Geophys 2019;57(1):106–45. https://doi.org/10.1029/2018rg000603.
[16] Smethurst JA, et al. Current and future role of instrumentation and monitoring in the performance of transport infrastructure slopes. Q J Eng Geol Hydrogeol 2017; 50(3):271–86. https://doi.org/10.1144/qjegh2016-080.
[17] Donohue S, Gavin K, Tolooiyan A. Geophysical and geotechnical assessment of a railway embankment failure. Near Surf Geophys 2011;9(1):33–44. https://doi.org/10.3997/1873-0604.2010040.
[18] Coughlan M, et al. Geological and geotechnical characterisation of soft Holocene marine sediments: a case study from the north Irish Sea. Eng Geol 2023;313: 106980. https://doi.org/10.1016/j.enggeo.2022.106980.
[19] Subramaniam P, et al. Modal analysis of Rayleigh waves using classical MASW-MAM approach: site investigation in a reclaimed land. Soil Dyn Earthq Eng 2020; 128:105902. https://doi.org/10.1016/j.soildyn.2019.105902.
[20] Wacquier L, et al. Time-Lapse monitoring of moisture induced landslide using surface waves at hollin hill landslide obsevatory. NSG2021 27th European Meeting of Environmental and Engineering Geophysics. European Association of Geoscientists & Engineers; 2021. 10.3997/2214-4609.202120163.
[21] Gunn D, et al. Aged embankment imaging and assessment using surface waves. Proceedings of the Institution of Civil Engineers-Forensic Engineering, 2016. **169** (4): p. 149-165.Doi: 10.1680/jfoen.16.00022.
[22] Donohue S, et al. Assessment of reservoir embankment dam condition using field and laboratory geophysical techniques. 1st Conference on Geophysics for Infrastructure Planning Monitoring and BIM. European Association of Geoscientists & Engineers; 2019. 10.3997/2214-4609.201902552.
[23] Anshu AK, et al. Seismic assessment of Itanagar city, Arunachal Pradesh, India: ELGRA studies incorporating spatially variable subsurface stratification derived from active MASW survey: AK Anshu et al. Journal of Earth System Science, 2025. **134**(3): p. 157.Doi: 10.1007/s12040-025-02606-1.
[24] Anshu AK, et al. Seismic hazard assessment frameworks in high-risk Indian regions: a methodological review and gap analysis with reference to Itanagar, India. Nat Hazard Rev 2026;27(3):03126003. https://doi.org/10.1061/NHREFO.NHENG-2606.
[25] He Z, Liu Q. Optical fiber distributed acoustic sensors: a review. J Lightwave Technol 2021;39(12):3671–86. https://doi.org/10.1109/jlt.2021.3059771.
[26] Bakulin A, Silvestrov I, Pevzner R. Surface seismics with DAS: an emerging alternative to modern point-sensor acquisition. Lead Edge 2020;39(11):808–18. https://doi.org/10.1190/tle39110808.1.
[27] Shatalin SV, Treschikov VN, Rogers AJ. Interferometric optical time-domain reflectometry for distributed optical-fiber sensing. Appl Opt 1998;37(24):5600–4. https://doi.org/10.1364/ao.37.005600.
[28] Masoudi A, Newson TP. High spatial resolution distributed optical fiber dynamic strain sensor with enhanced frequency and strain resolution. Opt Lett 2017;42(2): 290–3. https://doi.org/10.1364/ol.42.000290.

[29] Trafford A, et al. Distributed acoustic sensing for active offshore shear wave profiling. Sci Rep 2022;12(1):9691. https://doi.org/10.1038/s41598-022-13962-z.
[30] Ellmauthaler A, et al. Real-time DAS VSP acquisition and processing on single-and multi-mode fibers. IEEE Sens J 2020;21(13):14847–52. https://doi.org/10.1109/jsen.2020.3036930.
[31] Mateeva A, et al. Distributed acoustic sensing for reservoir monitoring with VSP. Lead Edge 2013;32(10):1278–83. https://doi.org/10.1190/tle32101278.1.
[32] Harris K, White D, Samson C. Imaging the Aquistore reservoir after 36 kilotonnes of CO2 injection using distributed acoustic sensing. Geophysics 2017;82(6):M81–96. https://doi.org/10.1190/geo2017-0174.1.
[33] Lindsey NJ, et al. Fiber-optic network observations of earthquake wavefields. Geophys Res Lett 2017;44(23):11792–9. https://doi.org/10.1002/2017gl075722.
[34] Walter F, et al. Distributed acoustic sensing of microseismic sources and wave propagation in glaciated terrain. Nat Commun 2020;11(1):2436. https://doi.org/10.1038/s41467-020-15824-6.
[35] Song Z, Zeng X, Thurber CH. Surface-wave dispersion spectrum inversion method applied to love and Rayleigh waves recorded by distributed acoustic sensing. Geophysics 2021;86(1):EN1–12. https://doi.org/10.1190/geo2019-0691.1.
[36] Song Z, et al. Sensing shallow structure and traffic noise with fiber-optic internet cables in an urban area. Surv Geophys 2021;42:1401–23. https://doi.org/10.1007/s10712-021-09678-w.
[37] Dou S, et al. Distributed acoustic sensing for seismic monitoring of the near surface: a traffic-noise interferometry case study. Sci Rep 2017;7(1):11620. https://doi.org/10.1038/s41598-017-11986-4.
[38] Zhan Z. Distributed acoustic sensing turns fiber-optic cables into sensitive seismic antennas. Seismol Res Lett 2020;91(1):1–15. https://doi.org/10.1785/0220190112.
[39] Thevenet E, et al. Assessing 3D slope condition with fibre optic seismic imaging using trains as sources. NSG 2024 30th European Meeting of Environmental and Engineering Geophysics. European Association of Geoscientists & Engineers; 2024. 10.3997/2214-4609.202420201.
[40] Ajo-Franklin JB, et al. Distributed acoustic sensing using dark fiber for near-surface characterization and broadband seismic event detection. Sci Rep 2019;9(1):1328. https://doi.org/10.1038/s41598-018-36675-8.
[41] Lai VH, et al. Passive seismic imaging of urban environments using distributed acoustic sensing. 2024. .
[42] Roshdy E, et al. Application of distributed acoustic sensing for active near-surface seismic monitoring. Sensors 2025;25(5):1558. https://doi.org/10.3390/s25051558.
[43] Ward W, Marsland A, Samuels S. Properties of the London clay at the ashford common shaft: in-situ and undrained strength tests. Geotechnique 1965;15(4):321–44. https://doi.org/10.1680/geot.1965.15.4.321.
[44] Powell J, Nash G, Bell P. GeoExposures: documenting temporary geological exposures in Great Britain through a citizen-science web site. Proc Geol Assoc 2013;124(4):638–47. https://doi.org/10.1016/j.pgeola.2012.04.004.
[45] Gasparre A, et al. The influence of structure on the behaviour of London Clay. Géotechnique 2007;57(1):19–31. https://doi.org/10.1680/geot.2007.57.1.19.
[46] Lim S, et al. Evaluation of soil pore-water salinity using a Decagon GS3 sensor in saline-alkali reclaimed tidal lands. Comput Electron Agric 2017;132:49–55. https://doi.org/10.1016/j.compag.2016.11.017.
[47] Kinzli K-D, Manana N, Oad R. Comparison of laboratory and field calibration of a soil-moisture capacitance probe for various soils. J Irrig Drain Eng 2012;138(4):310–21. https://doi.org/10.1061/(asce)ir.1943-4774.0000418.
[48] Khan Q, et al. A combined field and laboratory investigation into the moisture dependency of Vs for a clay-rich railway embankment fill. Eng Geol 2026:108702. https://doi.org/10.1016/j.enggeo.2026.108702.
[49] Donohue S, Long M. Assessment of an MASW technique incorporating discrete particle modelling. J Environ Eng Geophys 2008;13:57–68. https://doi.org/10.2113/JEEG13.2.57.
[50] Olafsdottir EA, Erlingsson S, Bessason B. Tool for analysis of multichannel analysis of surface waves (MASW) field data and evaluation of shear wave velocity profiles of soils. Can Geotech J 2018;55(2):217–33. https://doi.org/10.1139/cgj-2016-030.
[51] Nolet G, Panza GF. Array analysis of seismic surface waves: limits and possibilities. Pure Appl Geophys 1976;114(5):775–90. https://doi.org/10.1007/BF00875787.
[52] Maraschini M, et al. A new misfit function for multimodal inversion of surface waves. Geophysics 2010;75(4):G31–43. https://doi.org/10.1190/1.3436539.
[53] Maraschini M, Foti S. A Monte Carlo multimodal inversion of surface waves. Geophys J Int 2010;182(3):1557–66. https://doi.org/10.1111/j.1365-246x.2010.04703.x.
[54] Daley TM, et al. Field testing of modular borehole monitoring with simultaneous distributed acoustic sensing and geophone vertical seismic profiles at Citronelle. Alabama Geophys Prospecting 2016;64(5):1318–34. https://doi.org/10.1111/1365-2478.12324.
[55] Trafford A, et al. Distributed acoustic sensing for seismic surface wave data acquisition in an intertidal environment. Geophysics 2024;89(4):KS95–103. https://doi.org/10.1190/geo2023-0455.1.
[56] Vantassel JP, et al. Extracting high-resolution, multi-mode surface wave dispersion data from distributed acoustic sensing measurements using the multichannel analysis of surface waves. J Appl Geophys 2022;205:104776. https://doi.org/10.1016/j.jappgeo.2022.104776.
[57] Costley RD, et al. Spectral analysis of surface waves with simultaneous fiber optic distributed acoustic sensing and vertical geophones. J Environ Eng Geophys 2018;23(2):183–95. https://doi.org/10.2113/JEEG23.2.183.
[58] Galan-Comas G. Multichannel analysis of surface waves using distributed fiber optic sensors. 2015: Mississippi State University.
[59] Song Z, et al. Imaging shallow structure with active-source surface wave signal recorded by distributed acoustic sensing arrays. Earthq Sci 2018;31(4):208–14. https://doi.org/10.29382/eqs-2018-0208-4.
[60] Garofalo F, et al. InterPACIFIC project: Comparison of invasive and non-invasive methods for seismic site characterization. Part I: intra-comparison of surface wave methods. Soil Dyn Earthq Eng 2016;82:222–40. https://doi.org/10.1016/j.soildyn.2015.12.010.
[61] Smethurst J, Clarke D, Powrie W. Seasonal changes in pore water pressure in a grass-covered cut slope in London Clay. Géotechnique 2006;56(8):523–37. https://doi.org/10.1680/geot.2006.56.8.523.
[62] Fredlund DG, Morgenstern NR. Stress state variables for unsaturated soils. J Geotech Eng Div 1977;103(5):447–66. https://doi.org/10.1061/ajgeb6.0000423.
[63] Lu N, Likos WJ. Suction stress characteristic curve for unsaturated soil. J Geotech Geoenviron Eng 2006;132(2):131–42. https://doi.org/10.1061/(asce)1090-0241(2006)132:2(131).
[64] Fredlund D, Rahardjo H, Fredlund M. Unsaturated soil mechanics in engineering. Practice 2012. https://doi.org/10.1002/9781118280492.ch1.